Journal of Solid State Chemistry 184 (2011) 1415–1420

Contents lists available at ScienceDirect

Journal of Solid State Chemistry

journal homepage: www.elsevier.com/locate/jssc

Mixed surfactants-directed the mesoporous silica materials with various morphologies and structures

Huiming Lin [a], Fengyu Qu [a,*], Xiang Wu [a], Ming Xue [b], Guangshan Zhu [b], Shilun Qiu [b,*]

[a] Key Laboratory of Design and Synthesis of Functional Materials and Green Catalysis, Colleges of Heilongjiang Province and College of Chemistry and Chemical Engineering, Harbin Normal University, Harbin 150025, People's Republic of China

[b] State Key Laboratory of Inorganic Synthesis & Preparative Chemistry, Jilin University, Changchun 130012, People's Republic of China

ARTICLE INFO

Article history:
Received 16 November 2010
Received in revised form
23 March 2011
Accepted 26 March 2011
Available online 13 April 2011

Keywords:
Anionic surfactant
Cationic polymer
Mixed surfactants
Mesoporous silica materials

ABSTRACT

A new mixed surfactants system using alkyl carboxylic acids and quaternized poly[bis(2-chloroethyl) ether-alt-1,3-bis[3-(dimethylamino)propyl] urea] (PEPU) as the co-template was used to synthesize mesoporous silica materials with various morphologies and structures, including flakes, regular spheres, nanoparticles, and tube-spheres. The cationic polymer connected the anionic surfactant micelle to the anionic polysilicate species to induce the synthesis of the mesoporous silica materials. The structure and property of the surfactant and the cationic polymer determined the formation of mesoporous silica, and also had a signification influence on the morphology and structure of the final materials. To further explore the possible formation mechanism of these mesoporous materials, zeta potential was utilized to evaluate the interaction between the anionic surfactant and the cationic co-template. In addition, the structure, morphology, and porosity of these materials were characterized by powder X-ray diffraction (XRD), scanning electron microscopy (SEM), transmission electron microscopy (TEM), and N_2 adsorption–desorption measurements.

1. Introduction

Large surface area and pore volume, tunable pore sizes, and splendid morphologies and structures make the ordered mesoporous silica materials ideal for the application of bio-separation, adsorption, catalysis, and drug delivery [1–5]. Recently, many groups have been interested in using various surfactants to synthesize novel mesoporous materials for their special potential applications. The use of cationic surfactants [6], anionic surfactants [7–9], nonionic surfactants [10], neutral amine surfactants [11], block copolymer surfactants [12,13], and even the mixed surfactant systems have been reported in recent years. In the mixed surfactant systems, hydrophobic stuffing-surfactant [14,15], cosolute-surfactant [16], cationic–anionic surfactants [17–23], cationic–nonionic surfactants [24–26], and anionic–nonionic surfactants [27,28] have been studied. The assembly mechanism of the mixed surfactants system can be divided into two aspects: one is the solubilization of a hydrophobic agent, like 1,3,5-triethylbenzene (TMB) and 1,3,5-triisopropylbenzene (TIPB), inside the hydrophobic portion of the ordered surfactant mesophases. The other is the solubilization of a cosolute, such as alcohol and amphiphilic surfactant, in the palisade layer of the micelle formed by the surfactant. Both cases change the packing parameter g significantly ($g=V/al$, where V is the effective volume of the surfactant tail region, a is the effective head-group area at the micelle surface, and l is the surfactant tail length), which makes the mixed surfactants system always induce the special morphologies and structures.

TIPB was used as a filling agent to increase the pore size of SBA-15 with the pore diameter varying from 10 to 26 nm, even further to 50 nm with heterogeneous structure [15]. Ryoo et al. used cationic alkyltrimethylammonium bromides and poly (ethylene oxide) alkyl ethers surfactant mixtures as structure directing agents to prepare MCM-48 with high yield [24]. And the surfactant mixture of triblock copolymer P123 and *n*-butanol was also used to synthesize cubic $Ia\bar{3}d$ mesostructure with pore size ranging from 4 to 12 nm. The cubic phase domain is remarkably extended by controlling the amounts of butanol and silica source correspondingly [16]. Hollow spheres [23] and ellipsoidal nano-podlike mesoporous materials [22] were also templated from the alkyl trimethylammonium bromide (CTAB)/fluorocarbon surfactant systems. A mixture of CTAB and decanoic acid has been used as the structure directing agents in the synthesis of vesicle-like patterned mesoscopically ordered silica in the presence of toluene [21]. He et al. reported the synthesis of mesoporous silica nanomaterials with varied morphologies and pore structures, including nanospheres, nanoellipsoids, helical nanorods, and multi-lamellar nanovesicles using cetyltrimethylammonium bromide and sodium bis (2-ethylhexyl) sulfosuccinate as co-template [29].

* Corresponding authors. Fax: +86 451 88060653.
E-mail addresses: qufengyu@hrbnu.edu.cn, qufengyu2010@yahoo.cn (F. Qu).

0022-4596/$ - see front matter © 2011 Elsevier Inc. All rights reserved.
doi:10.1016/j.jssc.2011.03.043

Generally, in basic condition, the anionic surfactant cannot induce the synthesis of the mesoporous silica materials due to the unmatched interaction. The use of silane coupling agent to connect anionic surfactant to anionic silica species make anionic surfactant inducing the mesoporous silica materials come true [8,9]. In this paper, we try to introduce a cationic polymer, poly[bis(2-chloroethyl) ether-alt-1,3-bis[3- (dimethylamino)propyl]urea] (PEPU), as the new co-template to assist the anionic surfactant to induce the synthesis of the mesoporous silica materials. And, alkyl carboxylic acids with different chain lengths, including lauric acid, myristic acid, palmitic acid, and stearic acid were used as the anionic surfactants. The final meosporous materials with various morphologies and structures, such as flakes, regular spheres, nanoparticles, and tube-spheres were synthesized using the new mixed surfactants system.

2. Experimental

All chemicals were used as received without further purification. Poly[bis(2-chloroethyl) ether-alt-1,3-bis[3-(dimethylamino)propyl]urea], quaternized (62 wt% in H_2O), poly(diallyldimethylammonium chloride) (35 wt% in H_2O) and dodecyltrimethylammonium bromide (C12TAB) were purchased from Aldrich. Lauric acid, myristic acid, palmitic acid, and stearic acid were obtained from Tianjin Chemical Company. Tetraethyl orthosilicate (TEOS), sodium hydroxide (NaOH), and cetyltrimethyammonium bromide (C16TAB) were purchased from Beijing Chemical Company. Deionized water was used in all experiments.

Mixed surfactants system: in a typical synthesis, lauric acid (0.5 mmol) was dissolved in a solution containing H_2O (20 mL), ethanol (1 mL) and NaOH solution (3.1 mL, 0.2 M) at room temperature. PEPU aqueous solution (0.27 g, 10 wt %) was added and the mixture was stirred for 2 h. Then, 3 mL of TEOS was added and the mixture was continuously stirred for another 24 h. The solid samples were collected by centrifugation, washed with ethanol three times and dried at 60 °C. The template was completely removed by extraction in an ethanol–HCl mixture for 10 h, followed by calcination at 550 °C for 5 h in air condition. The synthetic details of other surfactant/polymer systems are summarized in Table 1.

The synthesis of MCM-41_{16}/MCM-41_{12} using C16TAB/C12TAB as the template has already been described in previous report [30]. In a typical procedure, a system with 3.00 g of C16TAB (2.54 g of C12TAB), 0.35 g of NaOH and 30 mL of H_2O was heated and stirred until a clear solution was obtained. Then 3 mL of TEOS was added and the system was continuously stirred for another 24 h at 60 °C (at room temperature for C12TAB system). The final sample was collected by filtration and washed with plenty of water. After dried at 60 °C overnight, the material was calcined to remove the template at 550 °C for 5 h.

Small-angle XRD diffraction (SAXRD) data were collected on a SIEMENS D5005 diffractometer with Cu $K\alpha$ radiation at 40 kV and 30 mA. Particle morphologies of these materials were determined by a scanning electron microscope (SEM) using JEOL-JSM-6700F operating at an accelerating voltage of 5 kV, and transmission electron microscope (TEM) images were recorded on JEOL 3010 with an acceleration voltage of 300 kV. Nitrogen adsorption–desorption was measured using a Micromeritics ASAP 2010 M adsorptometer. Before measured, the samples were degassed at 423 K for 12 h, and the measurement was carried out at 77 K. Specific surface areas and pore size distributions were calculated using Brunauer–Emmett–Teller (BET) and Barrett–Joyner–Halenda (BJH) models from the adsorption branches, respectively. The zeta potential of the precursor solution was evaluated by BROOKHAVEN ZetaPALS. FT-IR spectrometer (JASCOFT/IR-420) was used to record infrared spectra of the samples by the KBr method. Powder materials were pressed into a tungsten mesh grid and installed in an situ FT-IR transmission cell, and the samples were outgased in a vacuum system with a residual pressure of less than 3×10^{-4} Torr at ambient temperature.

Table 1
Synthesis condition and the characterization of the materials.

	Surfactant	PEPU (g)	Synthesis temperature (°C)	Pore size (nm)	Morphology
S-12	C_{11}–COOH	0.27	25	3.1	Flake
S-14	C_{13}–COOH	0.29	45	3.6	Sphere
S-16	C_{15}–COOH	0.31	60	4.0	Small particle
S-18	C_{17}–COOH	0.33	60	5.0	Tube-sphere
MCM-41_{12}	C12TAB		25	2.1	
MCM-41_{16}	C16TAB		60	2.9	

3. Results and discussion

SAXRD patterns of these products are depicted in Fig. 1. All the patterns show the peaks in small angle region, testifying the mesoporous structure of these materials. However, only one peak for all the samples suggests that the mesoporous structures are not ordered enough. With the increase of the chain length of the surfactants, the relevant peaks shift to the small angle region, implying the increase of pore sizes [30].

The morphologies of the samples were observed by SEM. Fig. 2 shows typical SEM images of S-12, S-14, S-16, and S-18. From Fig. 2a, S-12 displays flaky morphology with the average thickness of 200 nm. The morphology of S-14 (Fig. 2b) is a regular sphere with the particle size of about 250 nm. S-16 shows nanoparticles of about 50 nm in size. The nanoparticles agglomerate seriously, because of the small size, as shown in Fig. 2c. The rod-like particles of 2–5 μm in length and 300 nm in diameter can be found from S-18 (Fig. 2d). Interestingly, there is a layer of spheres with the diameter of 200 nm surrounding the rod. Each rod with the spheres around looks like a string of beads.

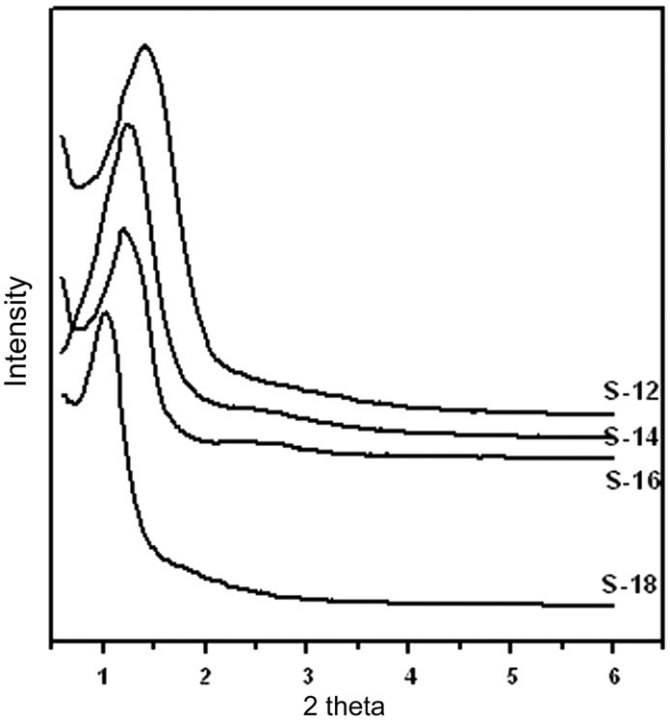

Fig. 1. SAXRD patterns of S-12, S-14, S-16, and S-18.

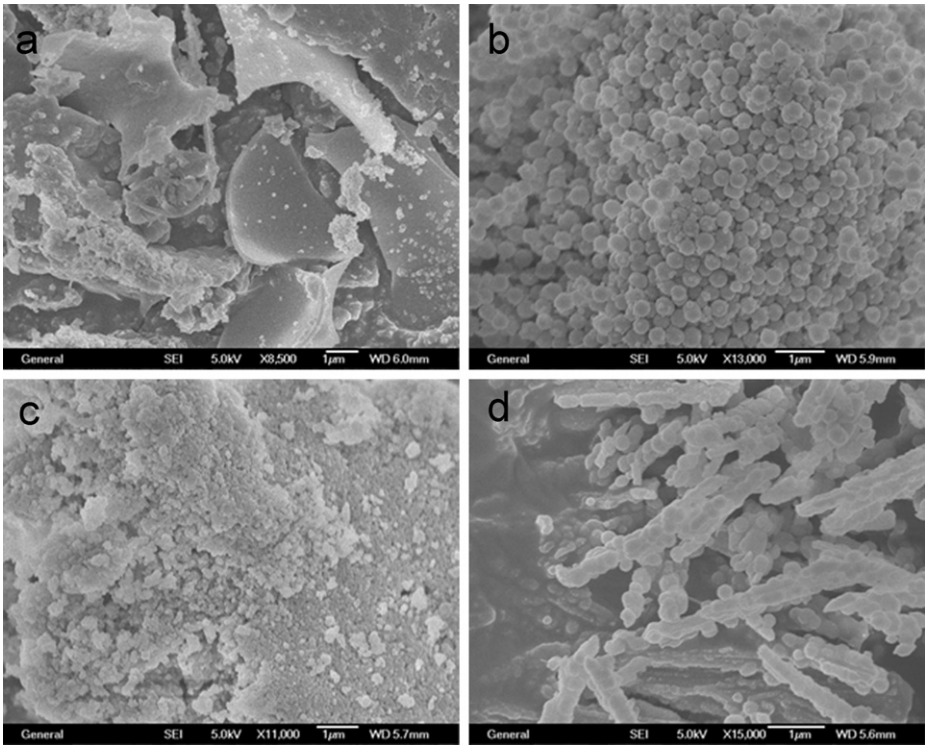

Fig. 2. SEM images: (a) S-12, (b) S-14, (c) S-16, and (d) S-18.

TEM studies were performed to further determine the pore structures of the products. The TEM images of S-12 (Fig. 3a and b) and S-14 (Fig. 3c and d) show the typical worm-like pore structure. From Fig. 3e and f, the typical TEM images recording along the [1 0 0], [1 1 0], and [1 1 1] directions suggested the body-centered cubic structure (space group $Im\bar{3}\ m$) of S-16. As shown in Fig. 3g–i, the rods (seen from the SEM images) are hollow with the inner diameter of about 100 nm, and the spheres are strung by the tube. Moreover, it can be found that some ends of the tube are open, while others are closed. The overgrowth of spheres closes the tube as the end closure. According to the TEM images, S-18 also possessed worm-like mesoporous structure.

From the images of SEM and TEM, each of the surfactants induces its special morphology/structure that may ascribe to the change of the packing parameter *g*. In our synthesis, the amount of PEPU is increased from 0.27 to 0.33 g (from S-12 to S-18) making the increase of head-group area at the micelle surface *a*. In addition, the chain length *l* of the surfactant increased from 1.73 to 2.25 nm (from lauric acid to stearic acid). Those effects induce the *g* value to decrease, which make for the mesoporous structure transfer from worm-like (S-12 and S-14) to cubic structure (S-16). And that is consistent with the former reports [31,32]. The formation of tube structures for S-18 is through the delicate interplay of both the mesoporous and vesicular structures (governed by the *g* value). The vesicular structure formed in solutions may serve as the "nucleation" site for the further deposition of a liquid-crystal mesostructure, thus leading to tubes with mesoporous wall structures [22,23,29].

The N_2 adsorption–desorption isotherm of S-18 (Fig. 4a) shows that a steep uptake at about $P/P_0=0.4$–0.7 together with a hysteresis loop, which is attributed to the presence of mesopore deriving from the surfactant template. As the amount of N_2 adsorption gradually increase following another hysteresis loop at about $P/P_0=0.9$–0.95 that is attributed to the spacing formed by the nanoparticles accumulations. The isotherm curves of other samples are similar to that of S-18. By comparing the isotherm curves of the samples, it can be found that S-14 has the most obvious hysteresis loop in the high relative pressure region. The possible reason is that, with more regular spherical morphology and larger particle size, the spacing formed by the nanoparticle accumulation of S-14 is more open and organized than that of other samples. The pore size distribution curves of the samples are shown in Fig. 4b. From the distribution curves, pore sizes are enlarged with the increase of the chain lengths of the surfactants. That is in accord with the results of XRD. The pore sizes of S-12, S-14, S-16, and S-18 are about 3.1, 3.6, 4.0, and 5.0 nm, respectively. And the surface area and pore volume are 469 $m^2\,g^{-1}$ and 0.37 $cm^3\,g^{-1}$, 352 $m^2\,g^{-1}$ and 0.33 $cm^3\,g^{-1}$, 331 $m^2\,g^{-1}$ and 0.30 $cm^3\,g^{-1}$, and 460 $m^2\,g^{-1}$ and 0.40 $cm^3\,g^{-1}$ for S-12, S-14, S-16, and S-18, respectively.

In order to testify that the PEPU was involved in the formation of the mesoporous phase, the FT-IR spectra were investigated. Carboxylate bands at 1638 and 1388 cm^{-1} are detected instead of the band at 1700 cm^{-1} corresponding to the carboxylic group (Fig. 5), indicating the deprotonation of lauric acid in the synthetic process. The characteristic absorption band at 1482 cm^{-1} can be attributed to the methyl groups of ammonium [33] and the N–H bending vibration at 1581 cm^{-1} is also observed. From the above observation, it can be affirmed that PEPU was involved in the formation of the mesoporous phase.

It is well known that, anionic surfactants cannot direct the synthesis of the mesoporous silica materials under the alkali condition because of the unmatched electrostatic force, which need a link to connect to the anionic silicate species. Herein, we used a cationic polymer (PEPU) to realize the target. Firstly, the anionic surfactant formed the micelle in aqueous solution, and then the PEPU surrounded the anionic micelle to form the co-micelle by the electrostatic force. In this condition, the surface of co-micelle exhibited positive charges deriving from the PEPU, which were enough to interact with the anionic silicates to induce the synthesis of the mesporous structure. Without the cationic polymer, no mesoporous structure was generated.

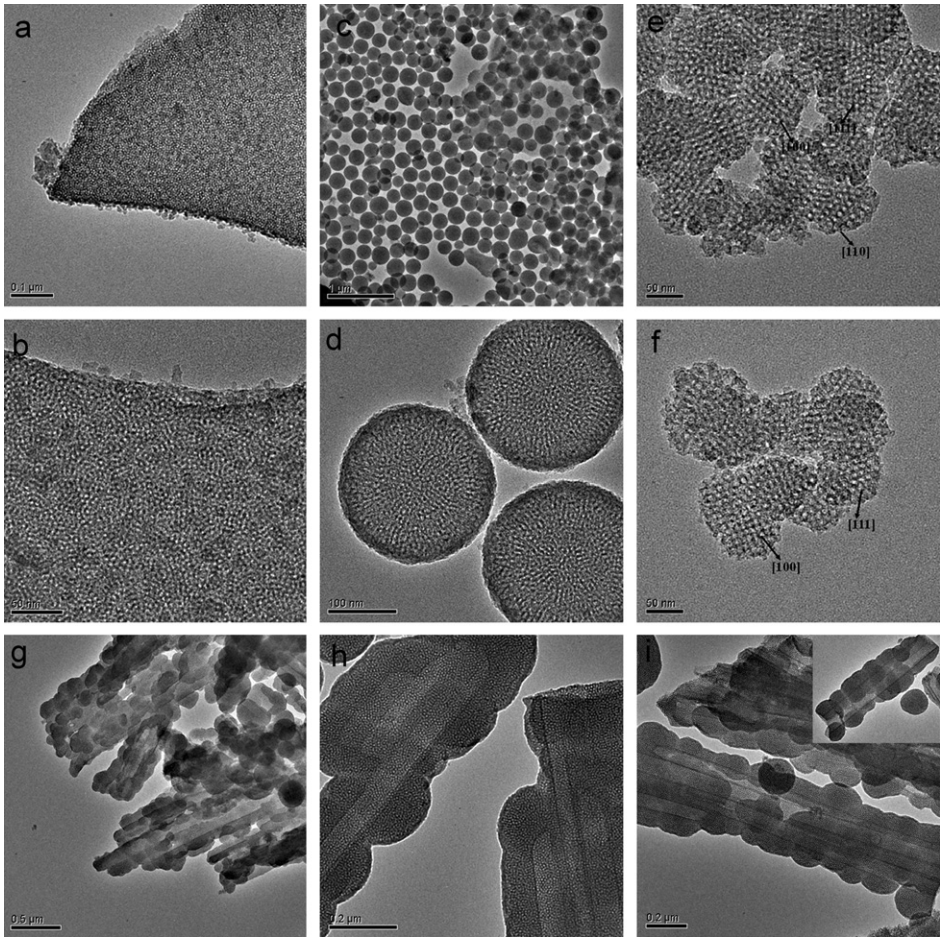

Fig. 3. TEM images: (a and b) S-12, (c and d) S-14 (e and f) S-16, and (g–i) S-18.

C16TAB and C12TAB were also used as the templates to synthesize the mesoporous materials (MCM-41_{16} and MCM-41_{12}) for comparison. From the data of N_2 adsorption–desorption, the relevant pore sizes of MCM-41_{16} and MCM-41_{12} are 2.9 and 2.1 nm (Fig. 6), respectively. With the similar chain length to C16TAB (2.22 nm) and C12TAB (1.83 nm), palmitic acid (2.15 nm) and lauric acid (1.73 nm) induced mesoporous materials with the pore size of 4.0 and 3.1 nm, respectively. The increase of 1 nm of pore size can be ascribed to the use of PEPU in the synthesis process. Different from the usual pore expanding agent (enlarge the size of the micelle from the inside), the use of PEPU increase the size of the micelle from the outside. PEPU coated round the anionic micelle to form co-micelle to induce the synthesis of the mesoporous materials. The above observations further testify that PEPU is involved in the mesoporous formation and act as a pore expanding agent in the synthesis process.

PEPU (Fig. 7) is a linear chain cationic polymer with good water-solubility. Another cationic polymer, poly(diallyldimethylammonium chloride) (PDDA) was also tried to use as the co-template in the mixed surfactant system. But it could not assist the anionic surfactant to form the uniform co-micelle. The system become precipitated, when too little PDDA (about 0.05 g 10 wt% solution) was added into the anionic surfactant solution. From the molecular structure of PDDA (Fig.7), it can be found that PDDA have the higher positive-charge density along the molecular chain. There is strong electrostatic force between PDDA and anionic surfactant making the co-micelle system suspension. Additionally, PDDA contains five-member-ring in the molecular structure that induces steric hindrance to connect to the anionic surfactant. So that it is difficult for PDDA to form a stable multilayer-pack co-micelle system. That is to say, PDDA is unsuitable to be used as the co-template in the mixed surfactants for mesoporous formation. From the above mentioned, it is can be found that the charge density and the structure of the polymer have a significant influence on the formation of the co-micelle system and the mesoporous structure as well.

The amount of co-template PEPU also plays an important role in the formation of the co-micelle. When PEPU is insufficient, there are too little cationic sites to connect the anionic silicates that make the mesoporous structure nonexistent. Contrarily, overmuch PEPU cationic polymer will assemble a large number of micelle to make the system precipitated [34–39], which is not suitable to induce the formation of the mesoporous materials. In our experiments, the optimization polymer/surfactant molar ratio is $R=0.45–0.51$. When the amount of PEPU exceeds the maximum, the co-micelle solution becomes precipitated. Whereas, the system keep homogeneous before the value of R reaches the optimization molar ratio.

With the aim of evaluating the interaction between anionic surfactant and cationic polymer to further understand the formation mechanism of the mesoporous materials, the zeta potential of the precursor solution was investigated (Fig. 8). From the zeta potential$\sim R$ curve of lauric acid, the initial anionic surfactant solution has the lowest zeta potential about -45.8 ± 2.3 mV responding to the negative charge on the surface of the anionic carboxylate micelle at the synthesis condition (pH=10). By adding the cationic PEPU, the interaction between PEPU and the anionic surfactant made a part of the carboxylate neutralized by

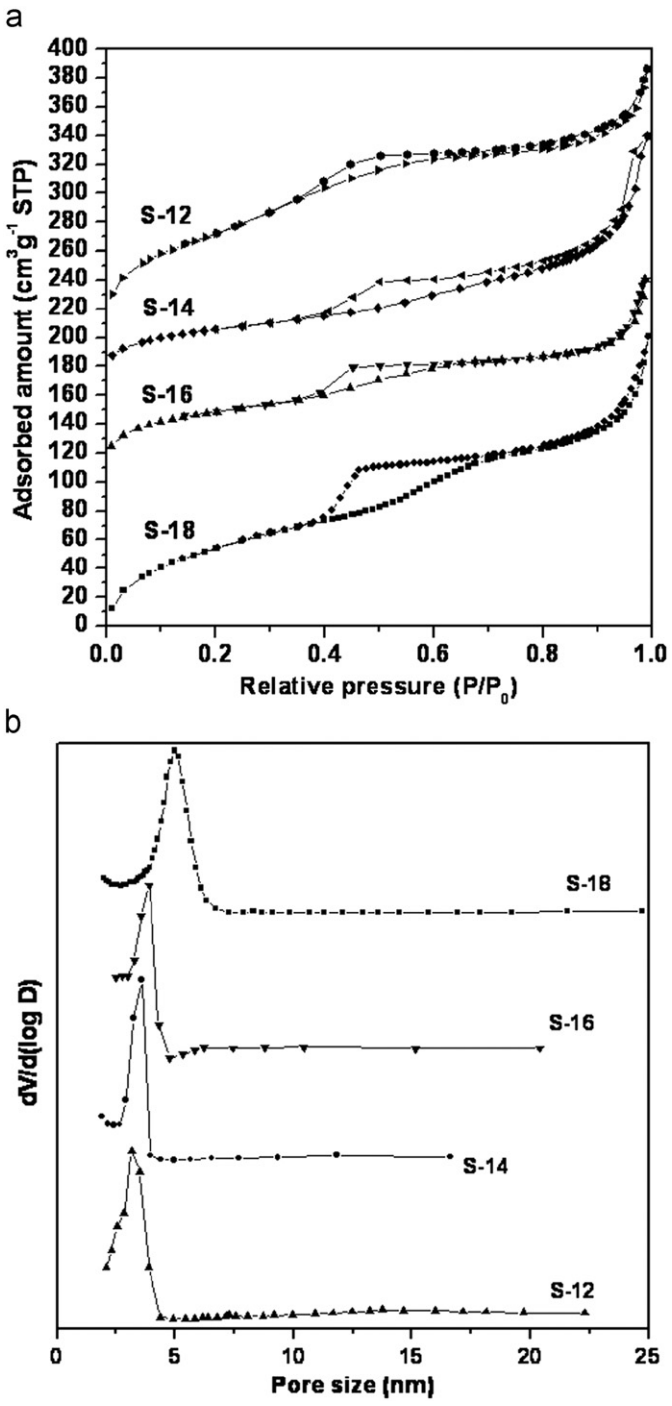

Fig. 4. (a) Nitrogen adsorption–desorption isotherms and (b) the corresponding pore size distributions of the samples.

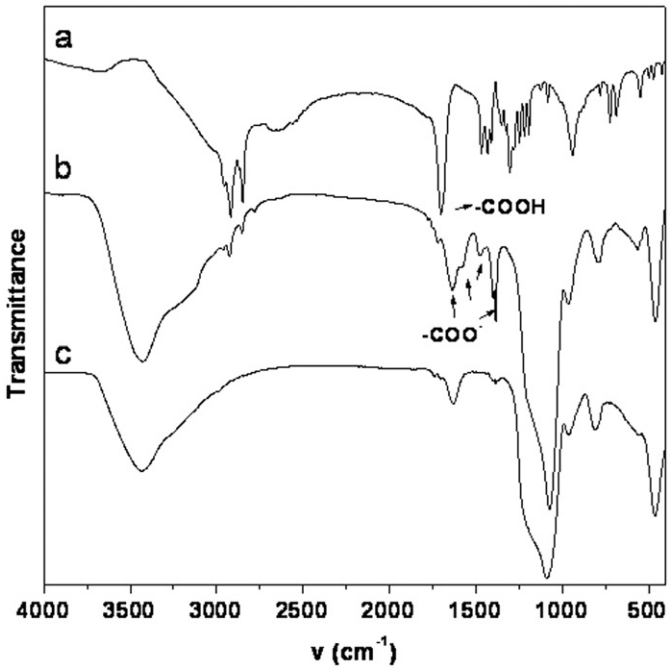

Fig. 5. FT-IR spectra of the materials: (a) lauric acid, (b) S-12, as-synthesis (without any post-treatment), and (c) S-12 (calcinations).

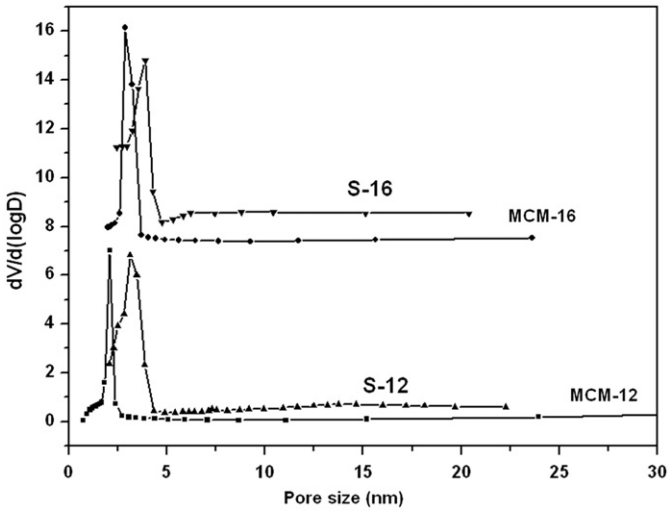

Fig. 6. Pore sizes of MCM-41$_{16}$, S-16, MCM-41$_{12}$, and S-12.

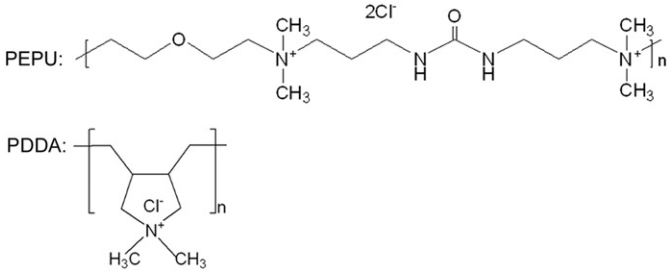

Fig. 7. Structure of the cationic polymer PEPU and PDDA.

the cationic PEPU, so that the zeta potential of the system increased obviously. When R value was increased to 0.45, the system had the highest zeta potential about -14.0 ± 1.5 mV. It is believed that, if the amount of the PEPU continued to increase, the system would possess positive zeta potential at last [39]. However, the precursor solution became precipitated, which were not suitable to induce the mesoporous structure as the template. From Fig.7, the zeta potential still remains negative, even the value of R increases to 0.45 (the synthesis condition). Nevertheless, the zeta potential just reflected the net charge of the co-micelle. Actually, a number of positive-charge (derived from PEPU) existed on the surface of the micelle under this condition, which was sufficient to connect to the anionic silicates and induced the mesoporous structure. So, the mesoporous structure was generated in the final materials.

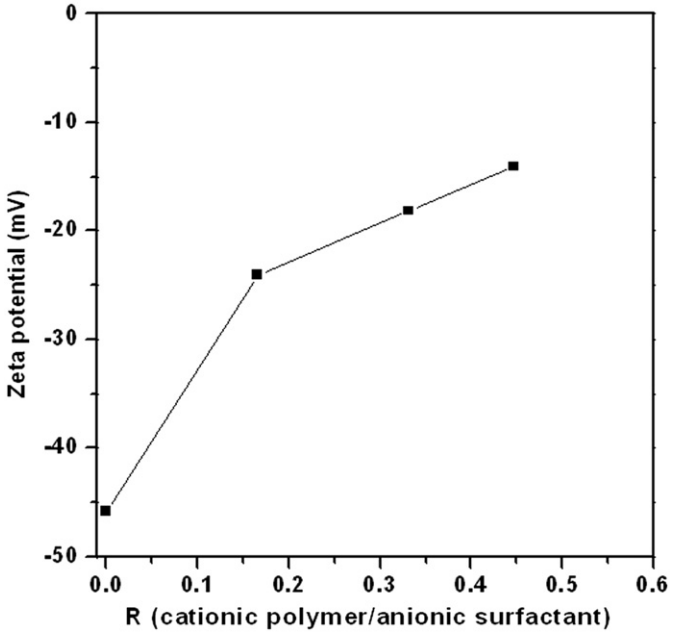

Fig. 8. Zeta potentials of the precursor solution (lauric acid) with different polymer/surfactant molar ratio *R*.

4. Conclusions

In conclusion, a cationic polymer PEPU was used to connect the anionic surfactants to the anionic polysilicate species to achieve the mesoporous materials. It is a new mixed surfactants system to synthesize the mesoporous materials, and it is also a development of the type $S^-N^+I^-$ route of the mesoporous formation. In this system, the synthesis of the mesopores was determined by many factors, such as the structure, charge density and amount of cationic polymer, the chain length of surfactants, and the molar ratio and interaction of the surfactant/polymer. The oppositely charged surfactant/polymer system is expected to extend to other surfactants and polymers to synthesize mesoporous materials with more special morphologies and structures. The different pore sizes, the various morphologies and structures make these materials possess potential applications in catalysis, separation, adsorption, control release, etc.

Acknowledgments

This work was supported by the National Natural Science Foundation of China (Grant no. 20871037, 20972036), Doctoral Initiation Fund of Harbin Normal University (KGB201006), and Innovation special fund of Harbin Science and Technology Bureau of China (2010RFXXS055).

References

[1] A. Corma, Chem. Rev. 97 (1997) 2373–2420.
[2] T.P. Corine, D. Brunel, S. Begu, B. Chiche, F. Fajula, D.A. Lerner, J.M. Devoisselle, New J. Chem. 27 (2003) 1415–1418.
[3] Y.F. Zhu, J.L. Shi, Y.S. Li, H.R. Chen, W.H. Shen, X.P. Dong, J. Mater. Res. 20 (2005) 54–61.
[4] N.K. Mal, M. Fujiwara, Y. Tanaka, Nature 421 (2003) 350–353.
[5] L.H. Chen, G.S. Zhu, D.L. Zhang, H. Zhao, M.Y. Guo, W. Shi, S.L. Qiu, J. Mater. Chem. 19 (2009) 2013–2017.
[6] C.T. Kresge, M.E. Leonowicz, W.J. Roth, J.C. Vartuli, J.S. Beck, Nature 359 (1992) 710–712.
[7] Q.S. Huo, D.I. Margolese, U. Ciesla, P.Y. Feng, T.E. Gier, P. Sieger, R. Leon, P.M. Petroff, G.D. Stucky, Nature 368 (1994) 317–321.
[8] S. Che, A.E. Garcia-Bennett, T. Yokoi, K. Sakamoto, H. Kunieda, O. Terasaki, T. Tatsumi, Nat. Mater. 2 (2003) 801–805.
[9] S. Che, Z. Liu, T. Ohsuna, K. Sakamoto, O. Terasaki, T. Tatsumi, Nature 429 (2004) 281–284.
[10] S.A. Bagshaw, E. Prouzet, T.J. Pinnavaia, Science 269 (1995) 1242–1244.
[11] P.T. Tanev, T.J. Pinnavaia, Science 267 (1995) 865–867.
[12] D.Y. Zhao, Q.S. Huo, J.L. Feng, B.F. Chmelka, G.D. Stucky, J. Am. Chem. Soc. 120 (1998) 6024–6036.
[13] D.Y. Zhao, J.L. Feng, Q.S. Huo, N. Melosh, G.H. Fredrickson, B.F. Chmelka, G.D. Stucky, Science 279 (1998) 548–552.
[14] J.S. Beck, J.C. Vartuli, W.J. Roth, M.E. Leonowicz, C.T. Kresge, K.D. Schmitt, C.T.-W. Chu, D.H. Olson, E.W. Sheppard, S.B. McCullen, J.B. Higgins, J.L. Schlenker, J. Am. Chem. Soc. 114 (1992) 10834–10843.
[15] L. Cao, T. Man, M. Kruk, Chem. Mater. 21 (2009) 1144–1153.
[16] T.W. Kim, F. Kleitz, B. Paul, R. Ryoo, J. Am. Chem. Soc. 127 (2005) 7601–7610.
[17] James G.C. Shen, J. Phys. Chem. B 108 (2004) 44–51.
[18] D. Chandra, A. Bhaumik, Ind. Eng. Chem. Res. 45 (2006) 4879–4883.
[19] F.X. Chen, L.M. Huang, Q.Z. Li, Chem. Mater. 9 (1997) 2685–2686.
[20] A. Lind, J. Andersson, S. Karlsson, P. Agren, P. Bussian, H. Amenitsch, M. Linden, Langmuir 18 (2002) 1380–1385.
[21] A. Lind, B. Spliethoff, M. Linden, Chem. Mater. 15 (2003) 813–818.
[22] S. Yang, X.F. Zhou, P. Yuan, M.H. Yu, S.H. Xie, J. Zou, G.Q. Lu, C.Z. Yu, Angew. Chem. Int. Ed. 46 (2007) 8579–8582.
[23] H. Djojoputro, X.F. Zhou, S.Z. Qiao, L.Z. Wang, C.Z. Yu, G.Q.J. Lu, Am. Chem. Soc. 128 (2006) 6320–6321.
[24] K. Suzuki, K. Ikari, H. Imai, J. Am. Chem. Soc. 126 (2004) 462–463.
[25] R. Ryoo, S.H. Joo, J.M. Kim, J. Phys. Chem. B 103 (1999) 7435–7440.
[26] Y. Han, D.F. Li, L. Zhao, J.W. Song, X.Y. Yang, C.J. Li, S. Wu, X.Z. Xu, X.J. Meng, K.F. Lin, F.S. Xiao, Angew. Chem. Int. Ed. 42 (2003) 3633–3637.
[27] D.H. Chen, Z. Li, C.Z. Yu, Y.F. Shi, Z.Z. Zhang, B. Tu, D.Y. Zhao, Chem. Mater. 17 (2005) 3228–3234.
[28] D.F. Li, X.Y. Guan, J.W. Song, Y. Di, D.L. Zhang, X. Ge, L. Zhao, F.S. Xiao, Colloids Surfaces A 272 (2006) 194–202.
[29] H.M. Chen, J.H. He, Chem. Commun. 37 (2008) 4422–4425.
[30] S.G. Li, M. Fang, W.Q. Pang, C.J. Che, C.M. Liu, Chin. J. Catal. 20 (1999) 161–165.
[31] P. Kipkemboi, A. Fogden, V. Alfredsson, K. Flodstrom, Langmuir 17 (2001) 5398–5402.
[32] J.M. Kim, Y. Sakamoto, Y.K. Hwang, Y.U. Kwon, O. Terasaki, S.E. Park, G.D. Stucky, J. Phys. Chem. B 106 (2002) 2552–2558.
[33] C.Q. Qin, Q. Xiao, H.R. Li, Int. J. Biol. Macromol. 34 (2004) 121–126.
[34] E.N. Savariar, S. Ghosh, D.C. González, S. Thayumanavan, J. Am. Chem. Soc. 130 (2008) 5416–5417.
[35] G. Nizri, A. Makarsky, S. Magdassi, Y. Talmon, Langmuir 25 (2009) 1980–1985.
[36] H.M. Lin, G.S. Zhu, J.J. Xing, B. Gao, S.L. Qiu, Langmuir 25 (2009) 10159–10164.
[37] G. Nizri, S. Magdassi, J. Colloid Interf. Sci. 291 (2005) 169–174.
[38] L.M. Bergstrm, U.R.Mikael Kjellin, Per M. Claesson, I. Grillo, J. Phys. Chem. B 108 (2004) 1874–1881.
[39] G. Nizri, S. Lagerge, A. Kamyshny, D.T. Major, S. Magdassi, J, Colloid Interf. Sci. 320 (2008) 74–81.